Nonlinear Impact of the Arctic Oscillation on extratropical surface air temperature

Hye-Young Son[1], Wonsun Park[2], Jee-Hoon Jeong[3], Sang-Wook Yeh[4], Baek-Min Kim[5], Minho Kwon[1] and Jong-Seong Kug[1]

[1]Korea Institute of Ocean Science and Technology , Ansan, Korea

[2]Helmholtz Centre for Ocean Research Kiel, Kiel, Germany.

[3]Department of Earth Sciences, University of Gothenburg, Gothenburg, Sweden

[4]Department of Environmental Marine Science, Hanyang University, Ansan, South Korea.

[5]Korea Polar Research Institute, Inchon, Korea

Corresponding author address: Dr. Jong-Seong Kug, Korea Institute of Ocean Science and Technology, Ansan, Korea. jskug@kiost.ac

Abstract

The Arctic Oscillation (AO) is the leading climate mode of sea level pressure (SLP) anomalies during cold season in the Northern Hemisphere. To a large extent, the atmospheric climate anomalies associated with positive and negative phases of the AO are opposite to each other, indicating linear impact. However, there is also significant nonlinear relationship between the AO and other winter climate variability. We investigate nonlinear impacts of the AO on surface air temperature (SAT) using reanalysis data and a multi-millennial long climate simulation. It is found that SAT response to the AO, in terms of both spatial pattern and magnitude, is almost linear when the amplitude of the AO is moderate. However, the response becomes quite nonlinear as the amplitude of the AO becomes stronger. First, the pattern shift in SAT depends on AO phase and magnitude, and second, the SAT magnitude depends on AO phase. In particular, these nonlinearities are distinct over the North America and Eurasian Continent. Based on the analyses of model output, we suggest that the nonlinear zonal advection term is one of the critical components in generating nonlinear SAT response, particularly over the North America.

1. Introduction

The Arctic Oscillation (AO) is the leading mode of atmospheric variability that can be expressed in terms of sea level pressure (SLP) anomalies during cold season using empirical orthogonal function (EOF) analysis [*Thompson and Wallace*, 1998; *Wallace*, 2000]. A characteristic spatial feature of the AO pattern is a strong zonal symmetric appearance with a primary action center over the Arctic and anomalies of opposite signs in the mid-latitudes (near 45°N) [*Deser*, 2000]. It has been widely reported that the AO significantly affects extreme weather events, such as cold air outbreak, frozen precipitation, and strong wind events over large area of the Northern Hemisphere [*Thompson and Wallace*, 2000; *Higgins et al.*, 2002; *Wettstein and Mearns*, 2002; *Jeong and Ho*, 2005]. In the negative (positive) phase of the AO, there are high (low) pressure anomalies over the Arctic and low (high) pressure anomalies over the Northern-Hemisphere extratropical oceans [*Gillett et al.*, 2002]. The polar jet encompassing a sub-polar region becomes weaker (stronger) which enables cold Arctic air to reach sub-Arctic and high-latitude regions more (less) easily during the negative (positive) AO phase [*Jeong and Ho*, 2005]. In particular, it has been recognized that very severe winters in recent years were closely associated with the frequent occurrence of negative AO phase of extremely high intensity [*Wang and Chen*, 2010].

Many studies have demonstrated that the AO is closely connected to mid- to high-latitude weather and climate from day-to-day variability to long-term trends. For instance, *Thompson and Wallace* [1998] and *Wang and Ikeda* [2000] found that the AO is closely related to surface air temperature (SAT) fluctuations in the Arctic and Eurasian Continent. *Rigor et al.* [2000] showed that the AO accounts for more than half of the SAT trends over Alaska, the eastern Arctic Ocean and Eurasia during the past two decades. *Jeong and Ho* [2005] and *Park et al.* [2010] suggested the occurrences of East Asian cold surge are dynamically associated

with the AO. Also, several studies reported that the temperature anomalies related to AO/NAO variability over Eurasian continent have been modulated in the inter-decadal scales [*Yu and Zhou*, 2004; *Li et al.*, 2005; *Xin et al.*, 2006; *Li et al.*, 2008]. Therefore, understanding the relation between climate variability and AO at different time scales, namely, from extreme events to decadal variability, is important for predicting future climate of the Northern Hemisphere.

The surface response patterns to the positive and negative phases of AO can be assumed to be opposite to each other and the amplitude of anomalies to be proportional to the strength of AO index (AOI), if the regional representation of AO impacts is linear. However, there are some evidences that suggest nonlinear characteristics of the AO impact on the Northern Hemisphere winter climate. Because AO is one of dominant climate variability in affecting the extra-tropical climate variation, the presence of the nonlinearity in AO impacts invokes considerable implication on understanding and predicting regional climate variation. For example, where the nonlinearity is strong, a simple linear approach does not work to utilize AO information. In particular, the dependency on AO magnitude will be required to understand regional climate variation in those regions. Several studies have reported that there is strong nonlinearity in AO impacts. *Higgins et al.* [2002] revealed that composite anomaly pattern of temperature extremes for negative AO in the US is considerably different from its counterpart for positive AO phase. *Shabbar and Bonsal* [2004] found a significantly higher frequency of cold spells over eastern Canada and an increased frequency of winter warm spells over the Canadian Prairies during positive AO winters (relative to negative AO winters). However, the changes in the frequency of warm spells between positive and negative AO phases are not exactly symmetric to those in the frequency of the cold spells. Furthermore, *Wu et al.* [2006] showed that a nonlinear projection of geopotential height at 500hPa and SAT anomalies with respect to the AOI exhibits asymmetric relationship over

North America.

Although these studies clearly showed the nonlinear impact of the AO, observational analysis by itself is limited to provide a related dynamics due to relatively short record length of observational data. To support the findings from observational analysis and explain the associated mechanism, we analyze the nonlinear impact of the AO in a multi-millennial climate model simulation and provide critical processes that invoke nonlinear structure changes due to AO impact. Our focus is given to the Northern Hemisphere, in particular over North America and Eurasia Continent.

Section 2 describes the data utilized, which include observational data and climate model output. The asymmetric patterns of SAT anomalies, with respect to AO phases and amplitude, and relevant dynamical processes are discussed in section 3. A brief summary and discussion are included in section 4.

2. Data and Model Output

We use monthly mean SLP, zonal and meridional winds, geopotential height and SAT at 2.5° by 2.5° resolution of the National Centers for Environmental Prediction/National Center for Atmospheric Research (NCEP/NCAR) reanalysis data [*Kalnay et al.*, 1996]. The data set includes 62 winters (December to February) for the period 1948/49 to 2009/10. Anomalies are defined by subtracting monthly mean climatology for the entire period.

To examine AO impacts and their nonlinearity, we analyze a multi-millennial long control simulation with the Kiel Climate Model (KCM), a fully coupled atmosphere-ocean-sea ice model. The KCM consists of the 5th-generation of ECHAM [ECHAM5; *Roeckner et al.*, 2003] atmospheric general circulation model (AGCM) and the Nucleus for European Modelling of the Ocean (NEMO) [*Madec*, 2008] ocean-sea ice general circulation model, which are coupled with the Ocean Atmosphere Sea Ice Soil version 3 (OASIS3; *Valcke*,

2006) coupler. The atmospheric model's resolution is T31 (approximately 3.75° by 3.75°) horizontally with 19 vertical levels and the ocean model's resolution is on average 1.3° with a latitudinal refinement to 0.5° toward the equator [*Park et al.*, 2009]. It is integrated for 5,000 years, and we use only the last 4,200 years, considering the first 800 years as the spin-up. *Semenov et al.* [2008] compared the recent trend of the North Atlantic Oscillation (NAO) in this simulation with the observation. Detailed information about the model setup and its general performance can be found in *Park et al.* [2009].

3. Results

The AO mode is obtained from the EOF analysis of winter (DJF) mean SLP anomalies north of 20°N from the observation (i.e., NCEP/NCAR Reanalysis) and the model simulation. Figure 1 shows the standardized leading EOF patterns of SLP and the regression fields of 500-hPa geopotential height (Z500) with respect to the calculated AOI during boreal winter. It is evident in the observation (Fig. 1a) and the model output (Fig. 1b) that the zonally symmetric dipole pattern prevails over the Arctic region and the mid-latitude, representing a typical Arctic-mid-latitude seesaw structure of the AO. The model captures well the pattern and magnitude of the observed AO, suggesting that the model has the ability in simulating observed AO characteristics. However, a systematic bias of the model simulation can be seen such that the simulated SLP anomalies over the North Pacific are too strong and expanded too much toward the Asian Continent compared to the observation.

The atmospheric circulation pattern, as represented by the projection of 500-hPa geopotential height onto the leading principal component (i.e., the AOI), also exhibits a similar dipole pattern (Figs. 1c and 1d). Likewise with the SLP anomalies, the negative geopotential height anomalies appear in the center of the Arctic region, and the positive anomalies are seen in extratropics. Overall, the model simulates the AO-related circulation

pattern reasonably. However, it tends that the simulated negative geopotential height anomalies over the Arctic region have a wider pattern and positive geopotential height anomalies over the North Pacific and North Atlantic Ocean are stronger, compared to the observation.

In order to investigate the impact of the AO on the Northern Hemisphere climate, we first perform composite analysis of SAT with respect to the AOI in the observation (Fig. 2) and model simulation (Fig. 3). We categorize the intensity of the AO using thresholds of 0.5 and 1.5 standard deviations of the AOI to define 'moderate' and 'strong' AO, respectively. During moderately negative AO phase (i.e., $-1.5\sigma < AOI < -0.5\sigma$), the composite SAT exhibits negative anomalies over northwestern Russia and eastern US, and positive anomalies over northeastern Canada to the Baffin Bay in the observation (Fig. 2a) and model simulation (Fig. 3a). When the AOI is moderately positive (i.e., $0.5\sigma < AOI < 1.5\sigma$), negative SAT field appears over the Baffin Bay and positive SAT anomalies are found over eastern US and northwestern Russia (Figs. 2b and 3b). However, there are some difference in the pattern of SAT anomalies between the observation and model. In Observation, the negative (positive) SAT anomalies exhibit from northwest Russia to northeast Russia during moderately negative (positive) AO phase (Figs. 2a and 2b). In the simulated model data, the negative (positive) SAT anomaly exhibits over northwestern (northeastern) Russia, and positive (negative) SAT anomaly over northeastern (northwestern) Russia during negative (positive) AO phase (Figs. 2d and 2e). Nevertheless, it tends that the simulated SAT composite is similar to its observational counterpart in terms of sign and magnitude. It is conceived from both of the observation and model (Figs. 2 and 3) that AO impacts on SAT are quite symmetric with respect to AO phase when the magnitude of the AO is moderate. For example, Figures 2c and 3c show the sum of observed SAT and simulated SAT anomalies for opposite AO phases, respectively. It is clear that the sum of the composite SAT anomalies is weak and, indicating

that the SAT anomalies exhibit symmetric responses to the AOI.

However, the AO impact on SAT variation becomes quite asymmetric as the AO magnitude becomes stronger. Composite SAT anomalies during strong AO phases (|AOI| > 1.5σ) reveal the asymmetric response of SAT anomalies to the AO phase (Figs. 2d,e,f and 3d,e,f). Overall, the magnitude of SAT anomalies becomes stronger in the whole North America and Eurasian continents in comparison with the moderate AO composites. In the observation, the SAT field gets colder during negative AO phase (Fig. 2d) and warmer for positive AO phase (Fig. 2e) over the both regions. Comparing Figure 2d with Figure 2e, the spatial pattern of SAT looks similar, but the magnitude of SAT is much bigger for the negative AO phase. This asymmetry is clear in the sum of positive and negative AO composites (Fig. 2f). It is interesting that the nonlinearity of AO impacts on SAT shows a dipole-like pattern over the North America continent. Unlike the case of moderate AO (Fig. 2c), the sum of the two composites shows distinctive signals over the whole Northern Hemisphere; in particular, the signal is strong over the Eurasian Continent and North America.

Because we used the monthly mean data in Figures 2 and 3, the sample numbers for the composites are not sufficient to reveal the nonlinearity of SAT response in case of the observation (Fig. 2). In order to increase the sample number, we also applied composite analyses based on observed daily mean data (Fig. 4). We found that the daily mean composites shows quite similar pattern to the monthly mean composite as shown in Figure 2, though the magnitude is slightly larger. Especially, the nonlinear part in SAT shows great similarity, indicating the results based on the monthly mean data are robust.

Next, we analyze in detail the climate model output and attempt to explain the mechanism that is involved in the generation of the nonlinearity of AO impacts. In the North America, the magnitude of SAT anomalies for strong negative AO phase (Fig. 3d) is larger than that for the strong positive AO phase (Fig. 3e); their spatial patterns are quite similar to

the observed ones (Figs. 2d and 2e). The sum of the composite mostly reflects the composite during the strong negative AO period. To a large extent, the SAT composites of the model are quite similar to those of the observation. In terms of the asymmetry, strong resemblance exists between the observation and the climate model simulation, particularly over North America, though the resemblance is weaker over the Eurasian Continent. The large asymmetry in North America commonly found in both the model and the observation, is thus quite interesting and needs to be examined further. Indeed, this finding is quite consistent with the results of *Wu et al.* [2006], which argued for a nonlinear relationship of SAT and Z500 associated with the AO over the North American winter.

3.1 North America

First, we focus on the asymmetry, i.e., the nonlinearity of AO impacts on SAT, over North America. As shown in Figure 3, the SAT anomalies over North America exhibit nearly a linear response to the AO phase of moderate magnitude; the SAT anomalies show nonlinear responses for stronger AO magnitude.

Since the observational data is not long enough to provide sufficient samples at different threshold categories of AO strengths (e.g., only 11 strong positive AO months for the analyzed period), we further analyze a long-term simulation of a climate model that provides enough samples. The AO events in the simulation are classified into 10 groups depending on AO magnitude, i.e., five different thresholds are applied to positive and negative phases of the AO. Figure 5 shows composites of simulated SAT anomalies over North America depending on different levels of threshold. Overall, negative SAT anomalies are predominant over North America during negative AO phase, and positive SAT anomalies are located in eastern Canada. These patterns are quite similar to the observed ones as shown in Figure 2.

Two interesting aspects can be found. One is the increased magnitude of SAT anomalies particularly for the stronger negative AO phase (Fig. 5). When AOI is weak, the spatial pattern and magnitude of SAT anomalies between the positive and negative phases are similar with different signs (i.e. linear). However, when the AOI is stronger (in this analysis above 1.5 standard deviation), the SAT responses to the positive and negative cases are not mirror images but provide strong loading in negative phase, which indicates the nonlinear response. The other is the westward shift of the anomalies as the AO magnitude becomes larger. As the AO magnitude becomes stronger, the positive and negative SAT anomalies tend to shift westward, compared to those of weak AO events. These features are quite consistent with the observed ones as shown in Figure 2.

The AO magnitude-dependent asymmetry is investigated further for the selected areas. We selected two areas where the nonlinearity is the strongest as shown in Figure 2: eastern Canada (EC; 50°-70°N, 60°-90°W) and northwestern America (NA; 45°-60°N, 100°-120°W). Figure 6 represents the relationship of area-averaged SAT anomalies vs. AOI in the observation and model simulation. The each dot represents the values from each composite as shown in Figure 5. The red line represents a possible linear response of SAT anomalies to the AOI based on a linear regression. If the dots are more in line with the red line, it indicates that the response of SAT anomalies to the AO is more linear. The observation shows a relatively weaker SAT response during positive AO phase in both EC (Fig. 6a) and in NA (Fig. 6c). In particular, when the magnitude of the AOI is 2.0 (standard deviation), the SAT anomalies for the negative AO is almost two times larger than that for the positive AO in NA (Fig. 6c). Also, the deviation from the linear regression becomes prominent as the AOI becomes larger. In spite of the limitation of the observational data due to small samples, this result well summarizes the nonlinear SAT response to the AO. In the model simulation,

similar patterns of nonlinear responses are found, and the signals are more robust presumably due to enough number of samples. In both of EC and NA, it is clearly seen that the SAT response is relatively weak in the positive phase of the AO (Fig. 6b), consistent with the observation (Fig. 6a). The magnitude of averaged SAT anomalies for the negative AO is almost two times larger than that for the positive AO.

Since the present climate model successfully captures the nonlinearity found in the observation over North America, analyses of model output may shed some light on what causes the nonlinear response. There are several dynamical processes that may contribute to the nonlinear responses. Firstly, the AO pattern itself exhibits the nonlinearity. Because the AO index is defined based on the EOF analysis of SLP, which is linear analysis, the detail structure of circulation can be different depending on AO magnitude. If the nonlinearity in circulation is strong, the nonlinear part of circulation directly results in the nonlinearity in SAT response to AO phases. In order to check the nonlinear part in the circulation, we carried out composites of SLP for strong positive and negative AO phases, respectively. Then we calculated the nonlinear part by adding two composites. Figure 7 shows the nonlinear part of SLP (contour) and SAT (shading) together. It is obvious that the positive (negative) SLP is matched with negative (positive) SAT in both observation and model simulation. The positive SLP pattern and associated circulation hardly explain the in-phase SAT anomalies. On the other hand, it is well known that the surface cooling leads to strengthening of the continental anticyclone over the continent. This implies the SAT anomalies lead to SLP anomalies [e.g. *Sung et al.*, 2011]. Also, we checked the relative magnitude of nonlinear component in SLP and SAT. Compared to their linear component, we found that the nonlinearity in SLP is much smaller than that in SAT (not shown). These results support that the nonlinear response of SAT cannot be fully explained by the nonlinearity in the circulation.

Instead of the nonlinear part of circulation, the nonlinear advection may explain the nonlinearity in SAT. We calculate the nonlinear term of temperature advection $\left(-u'\frac{\partial T'}{\partial x}-v'\frac{\partial T'}{\partial y}\right)$ for each AO event, and make composites according to AO magnitudes. The nonlinear term is calculated from the temperature and wind anomalies at 850hPa. Because the SAT pattern is quite similar to the pattern of 850hPa temperature (not shown), we can use the advection terms at 850hPa in order to reveal the cause of SAT nonlinearity.

Figure 8 shows the composite of nonlinear advection term during strong AO periods, derived from the observation and model output. The tripolar pattern of nonlinear advection in the observation is achieved during the strong negative AO phase, with negative advection over northwestern America, positive one over eastern Canada and negative one over the Baffin Bay (Fig. 8a). Note that the negative (positive) advection mostly appears to the west of the cold (warm) SAT anomalies (see Fig. 2). For positive AO events (Fig. 8b), the nonlinear advection term is relatively weak, but, interestingly, exhibits quite similar pattern to that for negative AO events. Therefore, the sum of the two composites, both showing nonlinearity, exhibits the tripolar pattern again (Fig. 8c).

In the model simulation (Figs. 8d-f), the nonlinear advection term exhibits similar tripolar pattern, though the pattern is slightly shifted to the east compared to the observed. In addition, the model tends to simulate relatively larger nonlinear advection term. In spite of the slight differences, the general features are quite similar. Overall, these spatial patterns of the nonlinear advection terms are quite similar to those indicating the nonlinear responses of SAT to the AO shown in Figures 3 and 4. This implies that the nonlinear temperature advection can be one of the critical factors in generating the nonlinear impacts of the AO.

In order to examine phase dependency of the nonlinear advection term, we calculate area-averaged nonlinear advection for the two boxes denoted in Figure 2f. We consider the

nonlinear zonal advection ($-u'\frac{\partial T'}{\partial x}$) and total nonlinear horizontal advection ($-u'\frac{\partial T'}{\partial x} - v'\frac{\partial T'}{\partial y}$) with respect to the AOI. The nonlinear meridional advection term ($-v'\frac{\partial T'}{\partial y}$) is overall weak compared to that of the zonal advection. There are only small differences between the nonlinear zonal advection and the total nonlinear horizontal advection (Fig. 9), indicating that the nonlinear zonal advection term ($-u'\frac{\partial T'}{\partial x}$) is the dominant term among the nonlinear advection terms. Therefore, we may simply use the nonlinear zonal advection term as a substitute for the nonlinear advection terms. However, there is quite significant difference in the second box between the nonlinear advection terms and zonal advection term when AOI is strong negative (Fig. 9b). This implies that the meridional advection can also be occasionally important for the nonlinear response in this region.

As shown in Figure 9a, nonlinear zonal temperature advection in eastern Canada is always positive regardless of AO phase. It is interesting that the nonlinear advection gets stronger as the magnitude of the AOI becomes larger. This is consistent with the stronger nonlinearity of SAT response to larger AO magnitude. The nonlinear advection term in the NA box, however, is always negative, and the magnitude of the term becomes larger as the AO magnitude becomes larger (Fig. 9b). The nonlinear advection term is particularly large for the strong positive AO phase, consistent with the relatively weak positive SAT anomalies shown in Figure 6d. These results support that the nonlinear advection may be a critical component in generating nonlinear impacts of the AO.

What causes the nonlinear advection in the two regions? In the North America, zonal wind anomalies largely exhibit westerlies (easterlies) for positive (negative) AO phase (Fig. 10). Contrasting to the zonally symmetric variation of zonal wind, SAT anomalies with respect to AO phase are quite asymmetric zonally due to the baroclinic features induced by the land-sea

contrast [*Thompson and Wallace*, 1998]. The zonal gradient of SAT anomalies ($\frac{\partial T'}{\partial x}$) also exhibits zonally asymmetric feature (Fig. 10). Consequently, during the negative AO phase the anomalous easterlies generate nonlinear warm (cold) advection over the EC region (northern US) in the west of positive (negative) temperature anomalies over the southern Baffin Bay (whole North America). As a result, the tripolar pattern of the nonlinear advection term (Fig. 8d) can appear. Note that the tripolar pattern of the nonlinear advection term is similar to that of the zonal temperature gradient. In a similar way, during the positive AO phase anomalous westerlies prevail, which leads to nonlinear warm (cold) advection over EC (northern US) in the east of positive (negative) temperature anomalies over northeastern America (the Baffin Bay). Therefore, the nonlinear advection during the positive AO phase exhibits a similar pattern to that during the negative AO phase. The temperature tendency due to such nonlinear advection processes can lead to asymmetric impacts with respect to AO phase.

In addition, because the nonlinear advection term is proportional to the product of temperature and zonal wind anomalies, its amplitude becomes considerably larger as the AO magnitude becomes larger. By definition, the nonlinear advection is the strongest in the outskirt of the warm/cold cores of SAT anomalies where the gradient is at its maximum. Such strong nonlinear advection tends to shift the SAT anomalies westward (eastward) pattern during strong negative (positive) AO phase, as seen in Figure 5.

3.2 Eurasian Continent

The nonlinear responses of SAT anomalies appear also over the Eurasian Continent in the observation (Fig. 2). In the observation, the SAT anomalies over East Asia exhibit the nonlinear impacts for strong AO magnitude, as the SAT anomalies over North America do

(Figs. 2c and 2f). However, it seems that the model has a systematic bias in simulating nonlinear impacts of the AO over the Eurasian Continent (see Figs. 3c and 3f). First, the overall pattern is shifted to the southwest compared to the observation, which can be related to stronger SLP and upper level circulation pattern over the Pacific shown in Figure 1b. In addition, strong negative SAT anomalies expand over Central Asia to East Asia in the observation (Fig. 2f); in the model simulation, they are considerably weaker over Central Asia, and become positive over East Asia (110°-130°E). Such biases are also found in the other climate models [*Xin* et al., 2008]

In spite of these obvious model biases, one may still find some interesting nonlinear impacts. With these model biases in mind, we apply a similar approach to the Eurasian region as done for the North America (section 3.1). Figure 11 shows SAT composite over the Eurasian Continent from the model. As the negative AO's magnitude becomes larger, the positive SAT anomalies over eastern Russia tend to expand further westward, compared to those for weak AO events. During the positive phase of the AO when the AO magnitude is moderate, the spatial pattern and magnitude of SAT anomalies look similar to those during positive phase. However, as the magnitudes of the AO becomes larger, the spatial pattern of SAT anomalies does not change much with increasing AO magnitude, in contrast to the case during negative phase of the AO. Also, the sum of SAT composites reflects well this relationship. As expected, the sum of SAT anomalies is quite weak for the period of weak AO magnitude. However, as the AO magnitude becomes stronger, negative (positive) SAT anomalies in Central East Asia (Eastern Russia) become larger (Figs. 11i, 11l and 11o).

We also examine the nonlinear term of temperature advection with respect to the AOI, in order to isolate the cause of nonlinear impacts of the AO on SAT anomalies over the Eurasian Continent (Fig. 12). We find two distinctive centers of large nonlinear advections in both AO phases: negative advection over Central Asia and positive advection over Eastern Russia.

Also, the spatial pattern of nonlinear advection for negative AO phase is similar to that for the positive AO phase. So, the sum of the two composites, representing the nonlinearity, shows a similar pattern to that of each composite. The nonlinear advection pattern in the model simulation is very similar to the nonlinear responses of SAT anomalies associated with the AO phase shown in Figure 11. This result means that the nonlinear zonal advection term is also an important factor for inducing the nonlinearity of SAT anomalies over Eurasian Continent. Nevertheless, the considerable difference in the nonlinear patterns of the observation and model indicates another dynamic process may be involved, which is not well produced in the model.

4. Summary and Discussion

We investigate the nonlinear relationship between the AO phase and SAT anomalies by using NCEP/NCAR reanalysis data and a multi-millennial control simulation with a climate model. Composite analyses show that SAT anomalies tend to linearly respond to weak and moderate AO events. However, as magnitude of the AO becomes stronger, distinctive nonlinear responses of SAT anomalies take place over North America and Eurasian Continent. We found from the analysis of long model simulation that the pattern of nonlinear impacts is quite consistent with that of nonlinear temperature advection. In addition, the nonlinear advection is larger when the AO magnitude is larger. These results suggest that the nonlinear advection can be one of the important processes in generating nonlinear responses of SAT anomalies to the AO.

While the model simulates reasonably well the AO impacts on SAT and its nonlinearity over the North America, those over the Eurasian Continent show some differences to the observed ones. In particular, the difference is distinct over the Siberian region. Observations show

stronger negative SAT anomalies over the Siberian region that expand to the northeast Asian region during the negative phase of AO, but such negative SAT anomalies are reduced in the model. On the other hand, model shows stronger positive anomalies during positive AO phase.

The distinct difference over the Siberian region can be linked to the Siberian High variability associated with the AO. During the negative AO phase, there is surface cooling over Siberia, which leads to the intensification of the Siberian High. The intensified Siberian High further enhances the surface cooling through the enhancements of snow-albedo feedback and radiative cooling, indicating a positive feedback. In addition, the intensified High induces anomalous northerly wind on the eastern side of the Siberian High, which leads to strong surface cooling. Since the surface cooling in turn induces anomalous high pressure, the Siberian High slowly expands to the east with the surface cooling, like thermal Rossby waves [*Sung et al.*, 2011]. However, during the positive AO phase this positive feedback and eastward expansion do not work effectively, the SAT anomalies are weak compared to those during the negative AO phase. Therefore, the observational nonlinearity over the Siberia can be related to the nonlinear response of the Siberian High and associated feedback.

In the model simulation, however, it seems the eastward expansion of the Siberian High and associated surface cooling are weaker during the negative AO phase. Note that in Figure 1d during negative (positive) AO phase the low (high) pressure system over the extratropical Pacific sector penetrates to the west too much, unlike in the observation. This biased low-pressure system can limit the eastward expansion of the Siberian High, which causes the bias in the nonlinear impact. In addition, we found there is a considerable warm bias in winter surface temperature over the Eurasian Continent (Fig. 13). The warm bias of the model may effectively block some physical processes, such as snow-albedo feedback, and contribute to further amplification of the Siberian High. A previous evaluation on the performance of

CMIP3 models in the simulation of AO pattern and related temperature anomalies showed similar model bias [*Xin et al.*, 2008].

In contrast to the Eurasian Continent, the model bias of the AO circulation pattern is relatively small over North America. In addition, the nonlinearity associated with the Continental High is weak due to the relatively small size of the continent, so the warm bias of surface temperature does not exist. Therefore, the nonlinear advection becomes a dominant factor in producing nonlinear impact over North America, and the model can simulate the nonlinearity reasonably well.

Reference

Deser, C. (2000), On the teleconnectivity of the "Arctic Oscillation", *Geophys. Res. Lett.*, *27*(6), 779-782.

Gillett, N. P., M. R. Allen, R. E. McDonald, C. A. Senior, D. T. Shindell, and G. A. Schmidt (2002), How linear is the Arctic Oscillation response to greenhouse gases?, *J. Geophys. Res.*, *107*(D3), 4022, doi:10.1029/2001JD000589.

Higgins, R. W., A. Leetmaa, and V. E. Kousky (2002), Relationships between climate variability and winter temperature extremes in the United States, *J. Clim.*, *15*(13), 1555-1572.

Jeong, J. H., and C. H. Ho (2005), Changes in occurrence of cold surges over east Asia in association with Arctic Oscillation, *Geophys. Res. Lett.*, *32*, L14704, doi:10.1029/2005GL023024.

Kalnay, E., et al. (1996), The NCEP/NCAR 40-year reanalysis project, *Bull. Am. Meteorol. Soc.*, *77*(3), 437-471.

Li, J., R. Yu, T. Zhou, and B. Wang (2005), Is there and early spring cooling shift downstream of the Tibetan Plateau?, *J. Clim.*, *18*(22), 4660-4668.

Li, J., R. Yu, and T. Zhou (2008), Teleconnection between NAO and climate downstream of the Tibetan Plateau, *J. Clim.*, *21*(18), 4680-4690.

Madec, G. (2008), NEMO ocean engine. *Note du Pole de modelisation No. 27*, pp.193, *Institut Pierre-Simon Laplace (IPSL)*, France.

Park, T. W., C. H. Ho, S. Yang, and J. H. Jeong (2010), Influences of Arctic Oscillation and Madden-Julian Oscillation on cold surges and heavy snowfalls over Korea: A case study for the winter of 2009-2010, *J. Geophys. Res.*, *115*, D23122, doi:10.1029/2010JD014794.

Park, W., N. Keenlyside, M. Latif, A. Stroh, R. Redler, E. Roeckner, and G. Madec (2009), Tropical Pacific Climate and Its Response to Global Warming in the Kiel Climate Model, *J. Clim.*, *22*(1), 71-92.

Rigor, I. G., R. L. Colony, and S. Martin (2000), Variations in surface air temperature observations in the Arctic, 1979-97, *J. Clim.*, *13*(5), 896-914.

Roeckner, E., and Coauthours (2003), The atmospheric general circulation model ECHAM5. Part Ⅰ: Model description, *Rep. 349*, pp. 127, Max Planck Institute for Meteorology, Hamburg, Germany.

Semenov, V. A., M. Latif, J. H. Jungclaus, and W. Park (2008), Is the observed NAO variability during the instrumental record unusual?, *Geophys. Res. Lett.*, 35, L11701, doi:10.1029/2008GL033273.

Shabbar, A., and B. Bonsal (2004), Associations between low frequency variability modes and winter temperature extremes in Canada, *Atmos. Ocean*, *42*(2), 127-140.

Sung, M. K., G. H. Lim, J. S. Kug, and S. I. An (2011), A linkage between the North Atlantic Oscillation and its downstream development due to the existence of a blocking ridge, *J. Geophys. Res.*, *116*, D11107, doi:10.1029/2010JD015006.

Thompson, D. W. J., and J. M. Wallace (1998), The Arctic Oscillation signature in the wintertime geopotential height and temperature fields, *Geophys. Res. Lett.*, *25*(9), 1297-1300.

Thompson, D. W. J., and J. M. Wallace (2000), Annular modes in the extratropical circulation. Part I: Month-to-month variability, *J. Clim.*, *13*(5), 1000-1016.

Valcke, S., Ed. (2006), OASIS3 user guide. *PRISM Tech. Rep. 3*, pp. 64, CERFACS, Toulouse, France.

Wallace, J. M. (2000), North Atlantic Oscillation/annular mode: Two paradigms - one phenomenon, *Q. J. R. Meteorol. Soc.*, *126*(564), 791-805.

Wang, J., and M. Ikeda (2000), Arctic oscillation and Arctic sea-ice oscillation, *Geophys. Res. Lett., 27*(9), 1287-1290.

Wang, L., and W. Chen (2010), Downward Arctic Oscillation signal associated with moderate weak stratospheric polar vortex and the cold December 2009, *Geophys. Res. Lett., 37*, L09707, doi:10.1029/2010GL042659.

Wettstein, J. J., and L. O. Mearns (2002), The influence of the North Atlantic-Arctic Oscillation on mean, variance, and extremes of temperature in the northeastern United States and Canada, *J. Clim., 15*(24), 3586-3600.

Wu, A. M., W. W. Hsieh, A. Shabbar, G. J. Boer, and F. W. Zwiers (2006), The nonlinear association between the Arctic Oscillation and North American winter climate, *Clim. Dyn., 26*(7-8), 865-879.

Xin, X., R. Yu, T. Zhou, and B. Wang (2006), Drought in late spring of south China in recent decades, *J. Clim., 19*(13), 3197-3206.

Xin, X. G., T. J. Zhou, and R. C. Yu (2008), The Arctic Oscillation in coupled climate models, *Chinese J. Geophys., 51*(2), 337-351.

Yu, R., and T. Zhou (2004), Impacts of winter-NAO on March cooling trends over subtropical Eurasia continent in the recent half century, *Geophys. Res. Lett., 31*, L12204, doi:10.1029/2004GL019814.

Figure 1. First EOF modes of (a) observed and (b) simulated sea level pressure (SLP) fields for the AO phase during boreal winter (DJF) in the Northern Hemisphere. Also given are the regressed 500-hPa geopotential height anomaly field for the AO phase of (c) observed and (d) simulated field during DJF.

Figure 2. Composite map of observed SAT anomalies for (a)-(c) moderate AO phase and (d)-(f) strong AO phase. (c) and (f) are the sums of (a+b) and (d+e) SAT composite for moderate and strong AO phase, respectively. Shading indicates the 90% confidence level.

Figure 3. The same as Figure 2 except for the simulated SAT composites.

Figure 4. The same as Figure 2 except for the observed daily mean composites

Figure 5. Composite map of simulated SAT during DJF for (left) negative and (middle) positive AO phases over the North America. The right panel is the sum of the left and center panels. Shading indicates the 90% confidence level.

Figure 6. Scatter plots of (left) observed and (right) simulated area-averaged SAT anomalies depending on AO phase. (a) and (b) are the results of EC (Eastern Canada: 50-70°N, 270-300°E). (c) and (d) show the results of NA (Northwestern America: 45-60°N, 240-260°E). The x-axis is AO phase, and the y-axis is SAT anomaly. The red line is a linear regression.

Figure 7. The nonlinear part of SAT (shaded) and SLP (contour) composites from (a) observation and (b) model simulation for relatively strong AO phase over the North America.

Figure 8. Composite maps of nonlinear advection term $\left(-\mathbf{u}'\frac{\partial \mathbf{T}'}{\partial \mathbf{x}} - \mathbf{v}'\frac{\partial \mathbf{T}'}{\partial \mathbf{y}}\right)$ for relatively strong AO phase over the North America. (a)-(c) are from the observations, and (d)-(f) are simulated output (K/s). (c) and (f) are the sums of nonlinear advection terms for

negative and positive AO phases, respectively.

Figure 9. Scatter plot of nonlinear zonal advection $\left(-u'\frac{\partial T'}{\partial x}\right)$ and total nonlinear advection $\left(-u'\frac{\partial T'}{\partial x}-v'\frac{\partial T'}{\partial y}\right)$ for the AO phase in the (a) eastern Canada and (b) northwestern America (K/s). The closed circle is the zonal nonlinear advection, and the open circle is the total nonlinear advection.

Figure 10. Composite map of wind anomaly (vector) and zonal temperature gradient (shading, 10^{-5}K/m) at 850 hPa for (a) strong negative and (b) strong positive AO phases.

Figure 11. The same as Figure 5, except over the Eurasian continent.

Figure 12. Composite maps of simulated nonlinear advection term $\left(-u'\frac{\partial T'}{\partial x}-v'\frac{\partial T'}{\partial y}\right)$ for relatively strong AO phase over the Eurasian continent. (c) is the sum of nonlinear advection terms for negative and positive AO phases.

Figure 13. Spatial distribution of SAT bias of the model simulation for December-January-February (DJF).

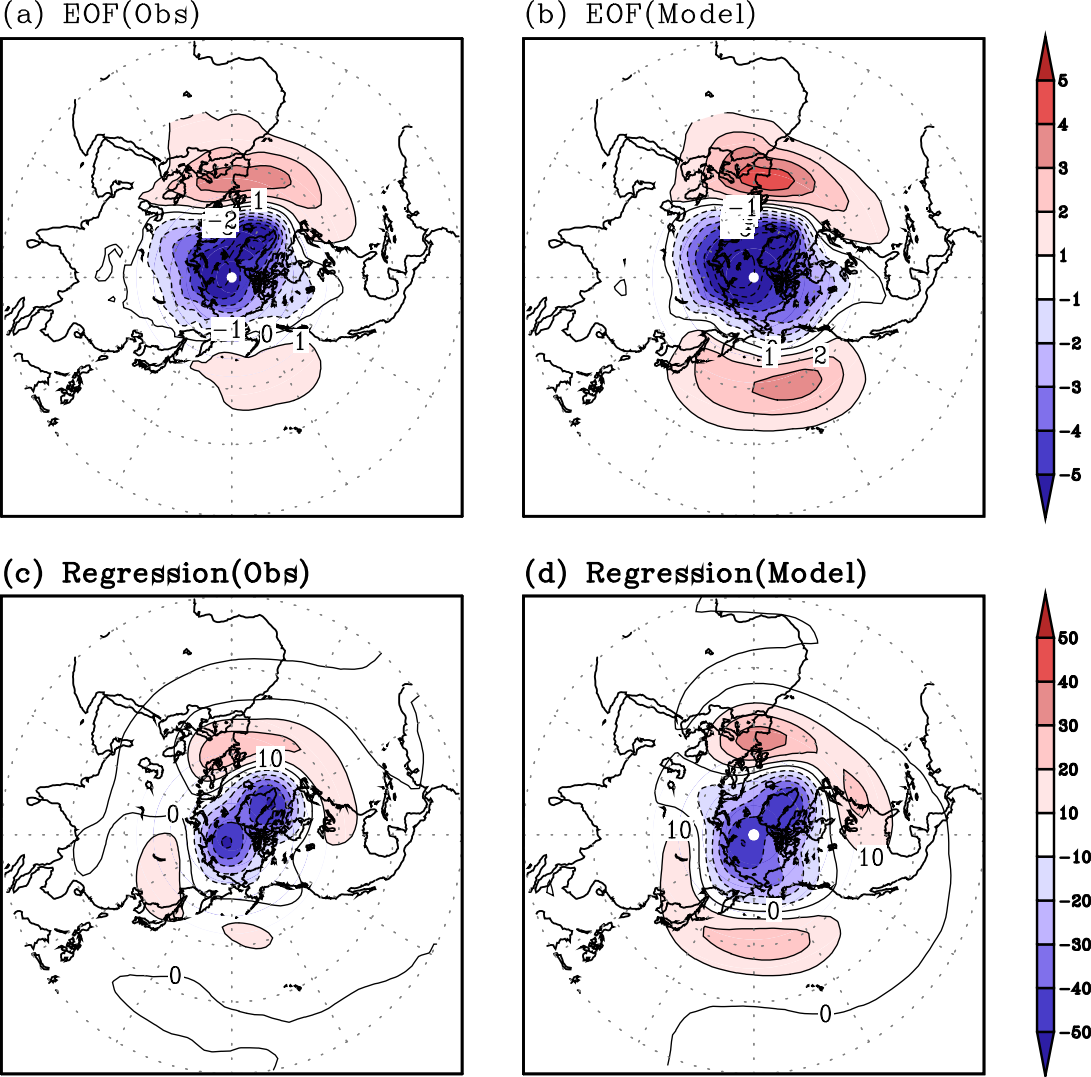
(a) EOF(Obs)
(b) EOF(Model)
(c) Regression(Obs)
(d) Regression(Model)
5
4
3
2
1
−1
−2
−3
−4
−5
50
40
30
20
10
−10
−20
−30
−40
−50

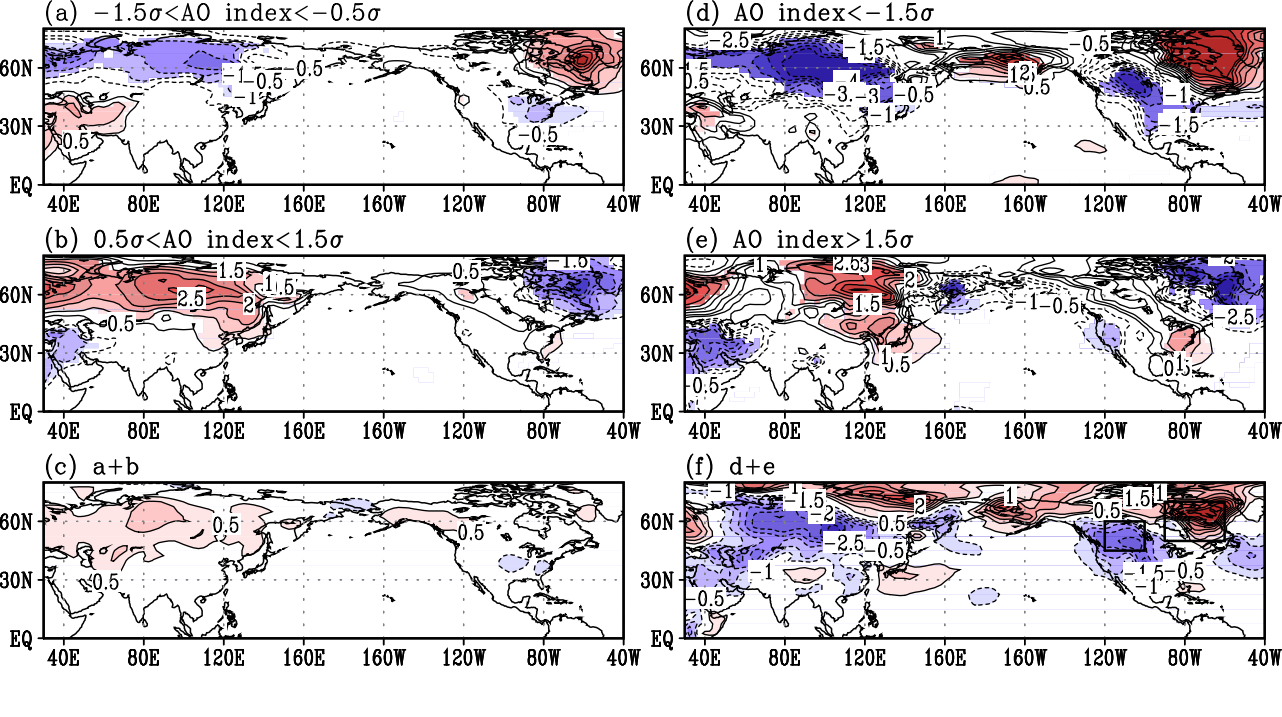
(a) −1.5σ<AO index<−0.5σ
(b) 0.5σ<AO index<1.5σ
(c) a+b
(d) AO index<−1.5σ
(e) AO index>1.5σ
(f) d+e
60N
30N
EQ
40E
80E
120E
160E
160W
120W
80W
40W
−4 −3.5 −3 −2.5 −2 −1.5 −1 −0.5 0.5 1 1.5 2 2.5 3 3.5 4

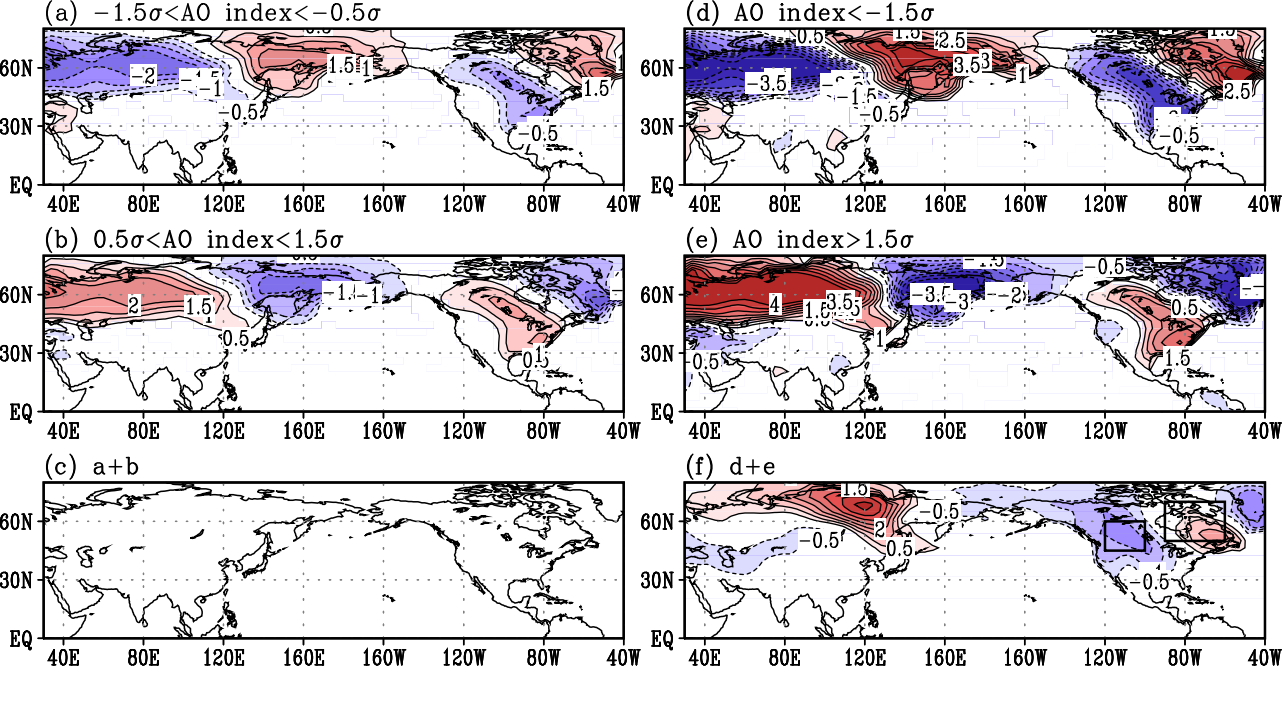
(a) −1.5σ<AO index<−0.5σ
(b) 0.5σ<AO index<1.5σ
(c) a+b
(d) AO index<−1.5σ
(e) AO index>1.5σ
(f) d+e
60N
30N
EQ
40E
80E
120E
160E
160W
120W
80W
40E
−4 −3.5 −3 −2.5 −2 −1.5 −1 −0.5 0.5 1 1.5 2 2.5 3 3.5 4

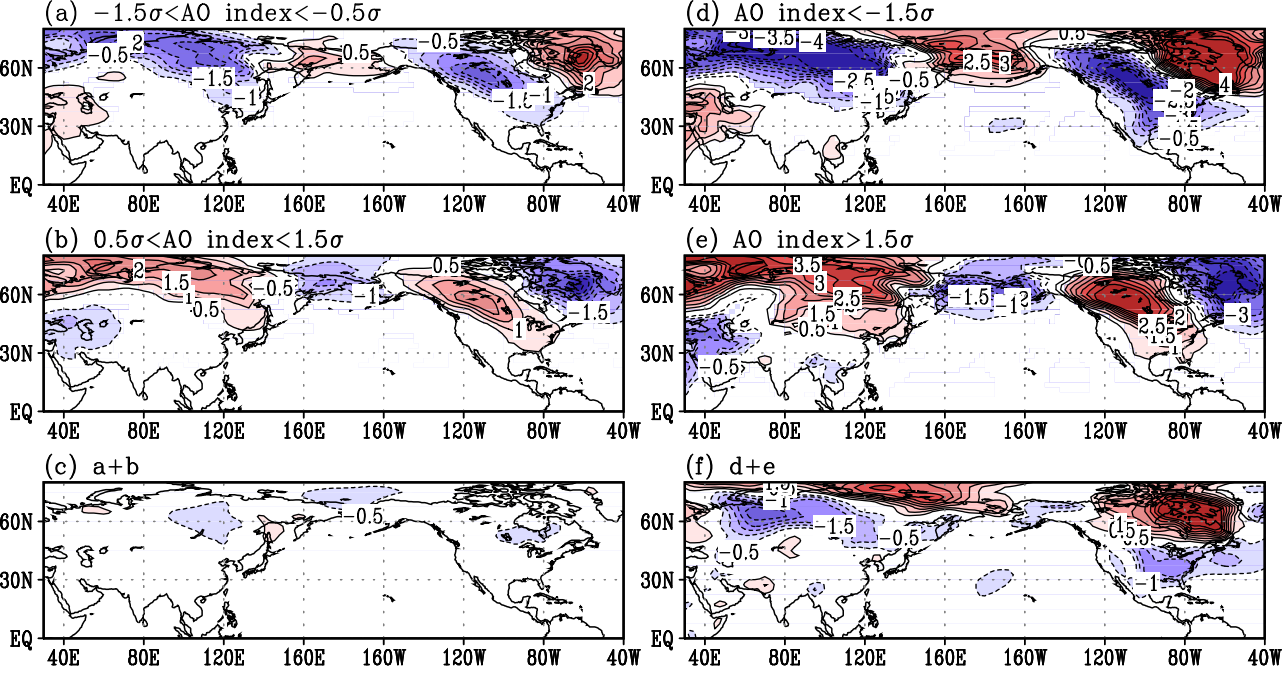
(a) −1.5σ<AO index<−0.5σ
(b) 0.5σ<AO index<1.5σ
(c) a+b
(d) AO index<−1.5σ
(e) AO index>1.5σ
(f) d+e
60N
30N
EQ
40E
80E
120E
160E
160W
120W
80W
40W
−4 −3.5 −3 −2.5 −2 −1.5 −1 −0.5 0.5 1 1.5 2 2.5 3 3.5 4

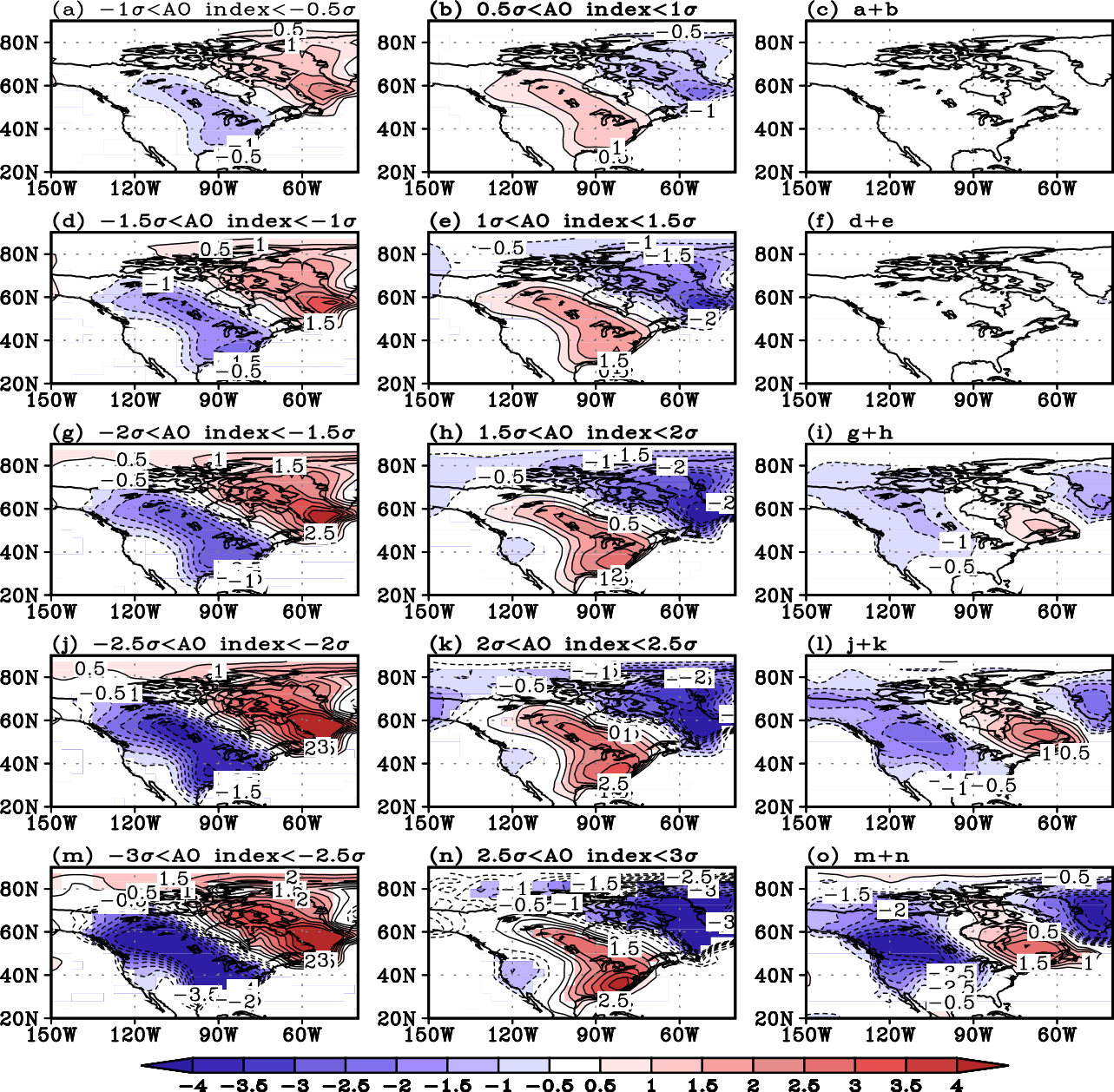
(a) −1σ<AO index<−0.5σ
(b) 0.5σ<AO index<1σ
(c) a+b
(d) −1.5σ<AO index<−1σ
(e) 1σ<AO index<1.5σ
(f) d+e
(g) −2σ<AO index<−1.5σ
(h) 1.5σ<AO index<2σ
(i) g+h
(j) −2.5σ<AO index<−2σ
(k) 2σ<AO index<2.5σ
(l) j+k
(m) −3σ<AO index<−2.5σ
(n) 2.5σ<AO index<3σ
(o) m+n
80N
60N
40N
20N
150W
120W
90W
60W
−4 −3.5 −3 −2.5 −2 −1.5 −1 −0.5 0.5 1 1.5 2 2.5 3 3.5 4

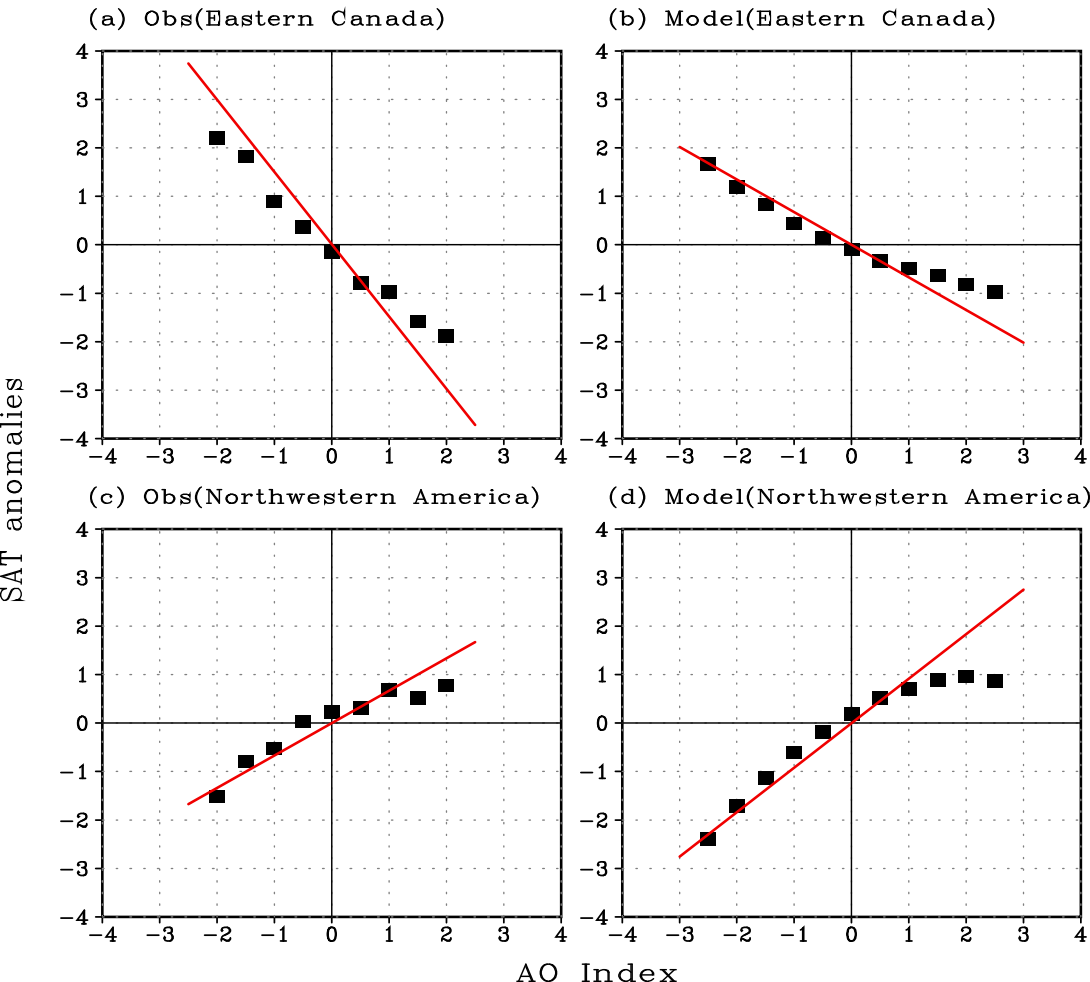
(a) Obs(Eastern Canada)
(b) Model(Eastern Canada)
(c) Obs(Northwestern America)
(d) Model(Northwestern America)
SAT anomalies
AO Index

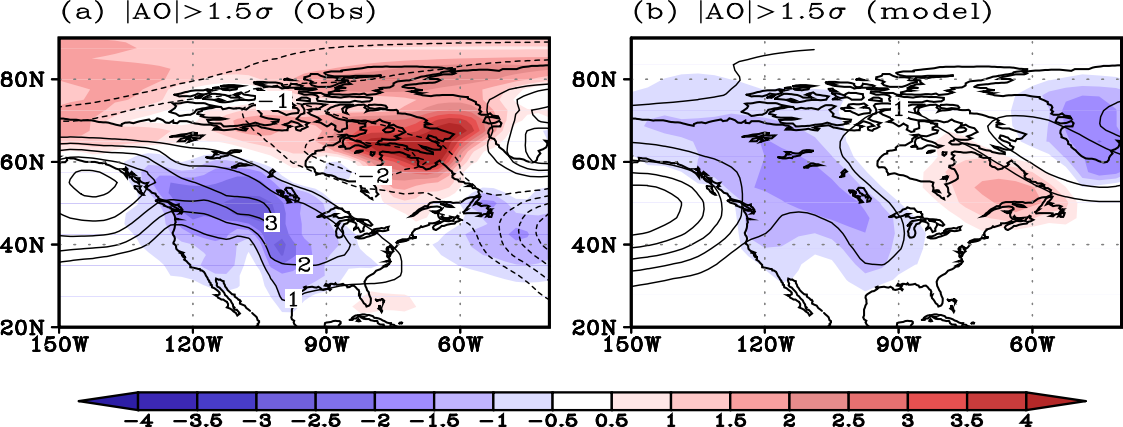
(a) |AO|>1.5σ (Obs)
(b) |AO|>1.5σ (model)
80N
60N
40N
20N
150W
120W
90W
60W
−1
−2
3
2
1
−4 −3.5 −3 −2.5 −2 −1.5 −1 −0.5 0.5 1 1.5 2 2.5 3 3.5 4

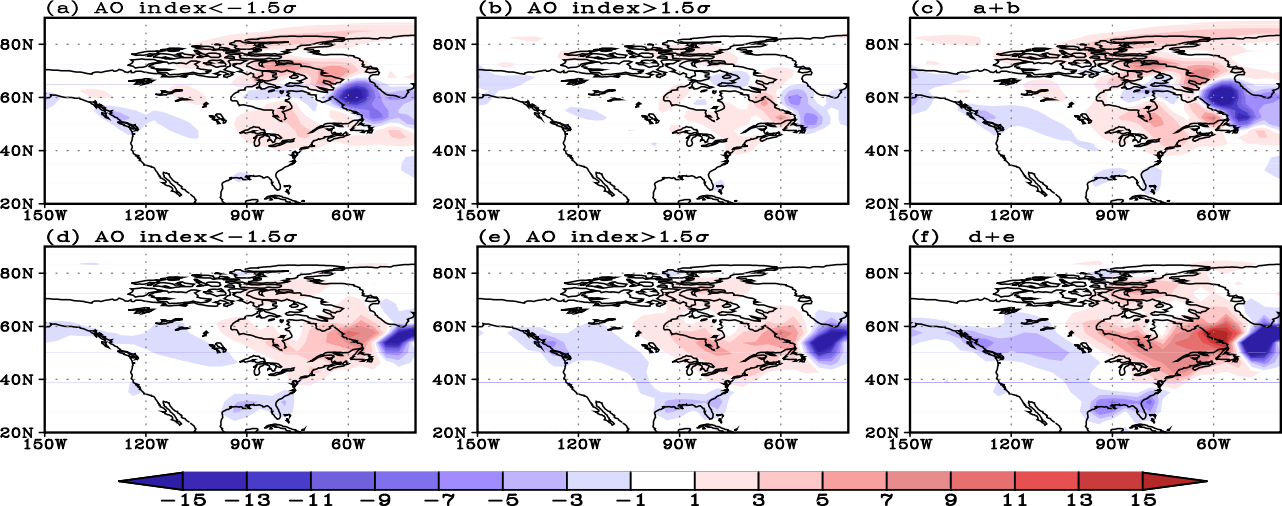
(a) AO index<−1.5σ
(b) AO index>1.5σ
(c) a+b
(d) AO index<−1.5σ
(e) AO index>1.5σ
(f) d+e
80N
60N
40N
20N
150W
120W
90W
60W
−15 −13 −11 −9 −7 −5 −3 −1 1 3 5 7 9 11 13 15

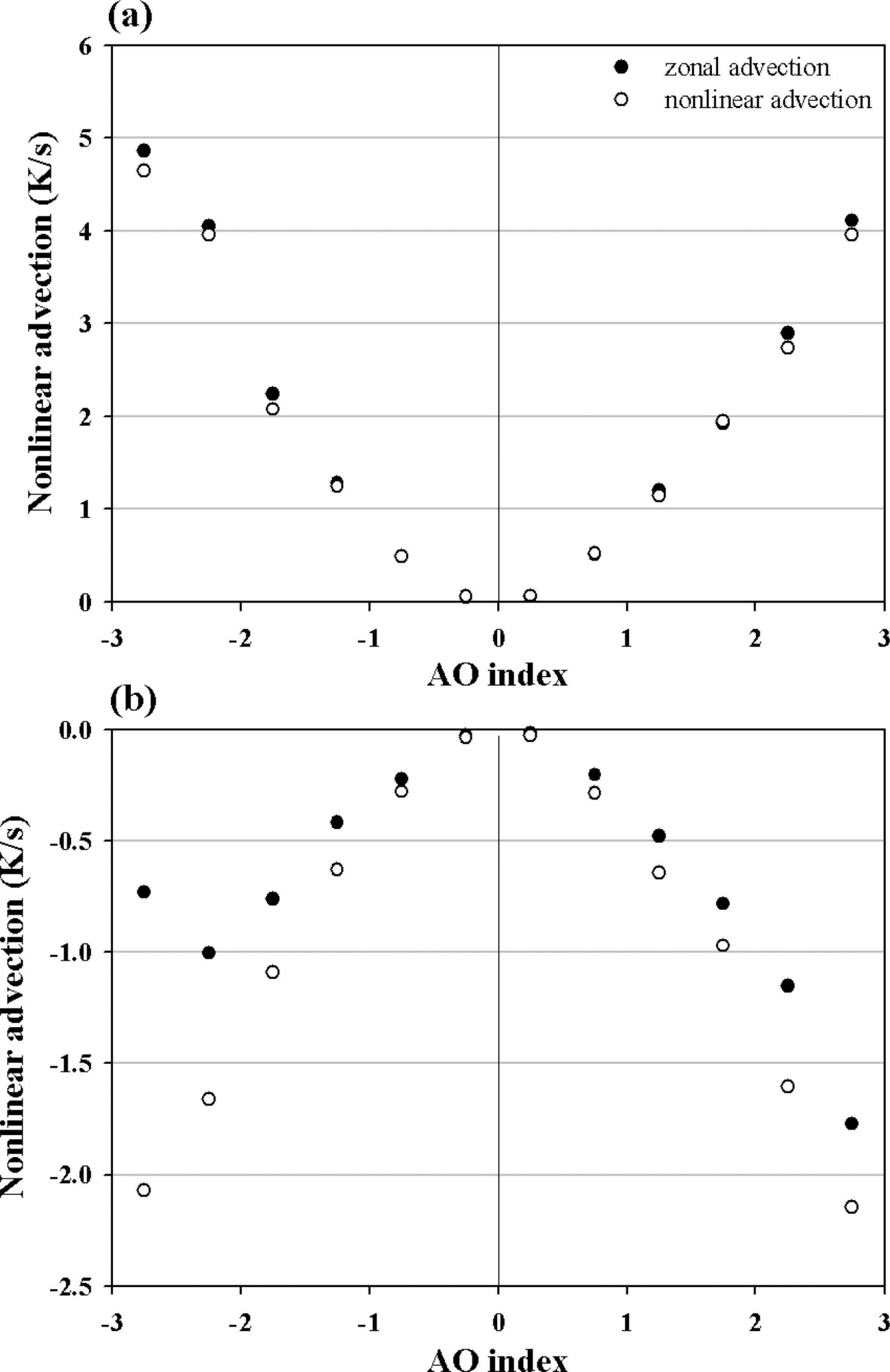
(a)
zonal advection
nonlinear advection
Nonlinear advection (K/s)
6
5
4
3
2
1
0
-3
-2
-1
0
1
2
3
AO index
(b)
Nonlinear advection (K/s)
0.0
-0.5
-1.0
-1.5
-2.0
-2.5
-3
-2
-1
0
1
2
3
AO index

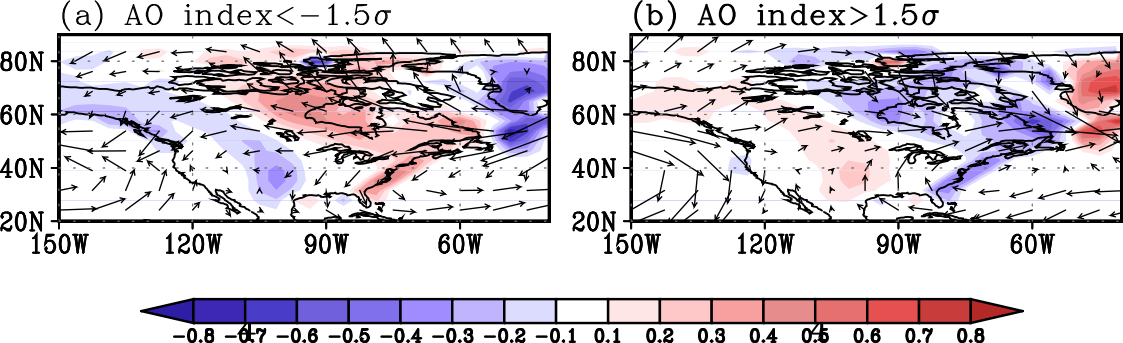
(a) AO index<−1.5σ
(b) AO index>1.5σ
80N
60N
40N
20N
150W
120W
90W
60W
−0.8 −0.7 −0.6 −0.5 −0.4 −0.3 −0.2 −0.1 0.1 0.2 0.3 0.4 0.5 0.6 0.7 0.8

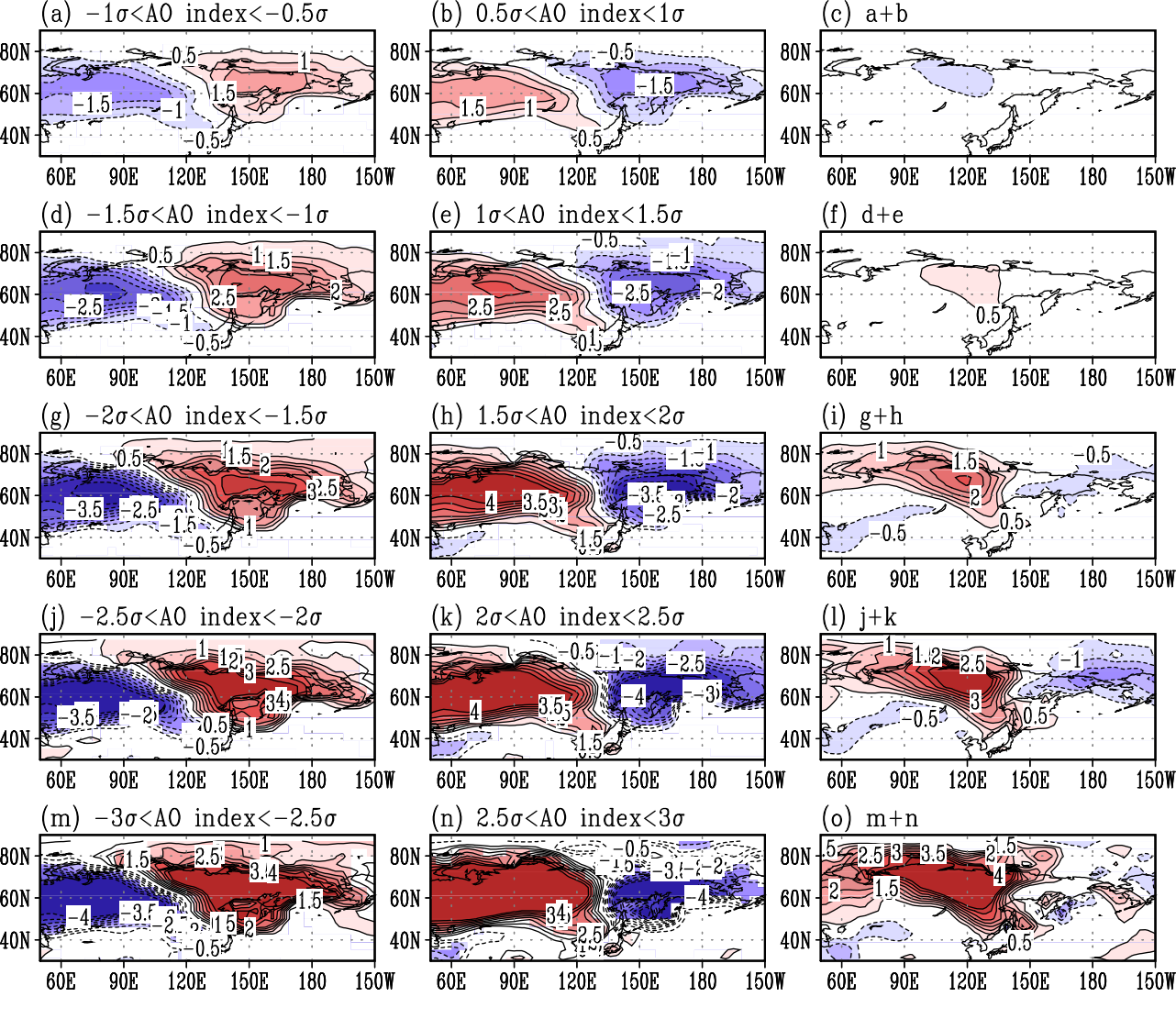
(a) −1σ<AO index<−0.5σ
(b) 0.5σ<AO index<1σ
(c) a+b
(d) −1.5σ<AO index<−1σ
(e) 1σ<AO index<1.5σ
(f) d+e
(g) −2σ<AO index<−1.5σ
(h) 1.5σ<AO index<2σ
(i) g+h
(j) −2.5σ<AO index<−2σ
(k) 2σ<AO index<2.5σ
(l) j+k
(m) −3σ<AO index<−2.5σ
(n) 2.5σ<AO index<3σ
(o) m+n
80N
60N
40N
60E
90E
120E
150E
180
150W
−4 −3.5 −3 −2.5 −2 −1.5 −1 −0.5 0.5 1 1.5 2 2.5 3 3.5 4

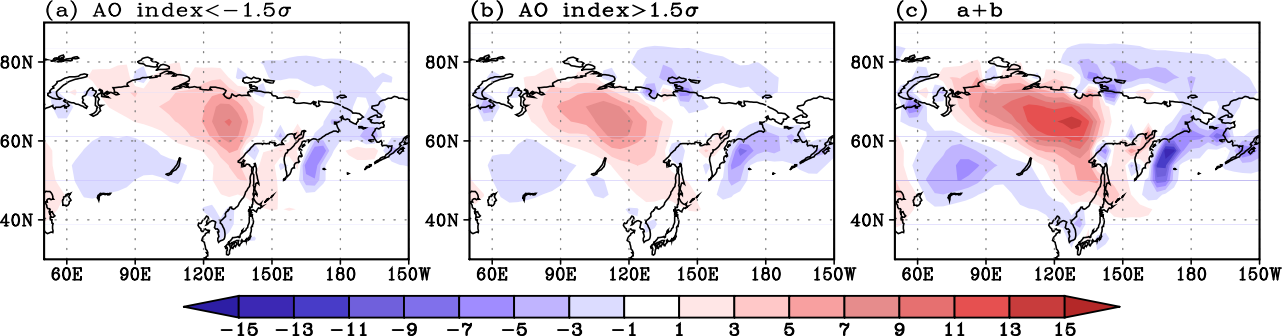
(a) AO index<−1.5σ
(b) AO index>1.5σ
(c) a+b
80N
60N
40N
60E
90E
120E
150E
180
150W
−15 −13 −11 −9 −7 −5 −3 −1 1 3 5 7 9 11 13 15

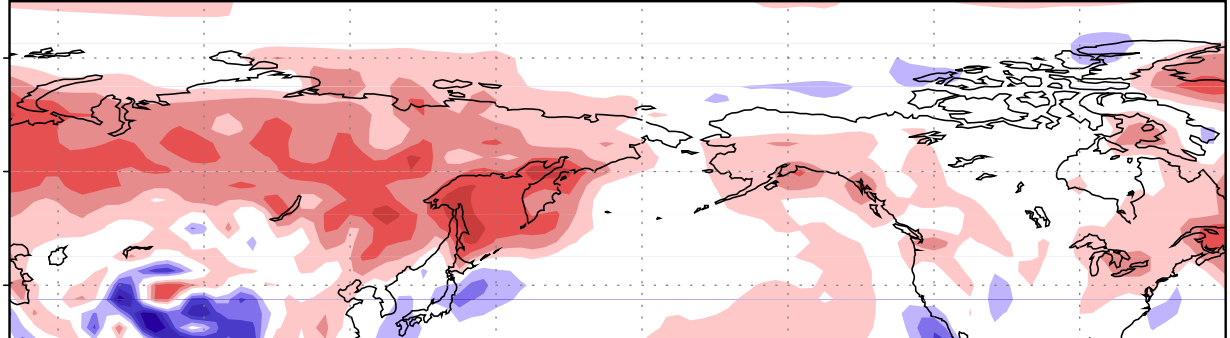
80N
60N
40N
60E
90E
120E
150E
180
150W
120W
90W
60W
−10
−8
−6
−4
−2
2
4
6
8
10